

# SANDIA REPORT

SAND96-1019 • UC-404  
Unlimited Release  
Printed December 1996

## Characterization of Microstructure and Crack Propagation in Alumina Using Orientation Imaging Microscopy (OIM)

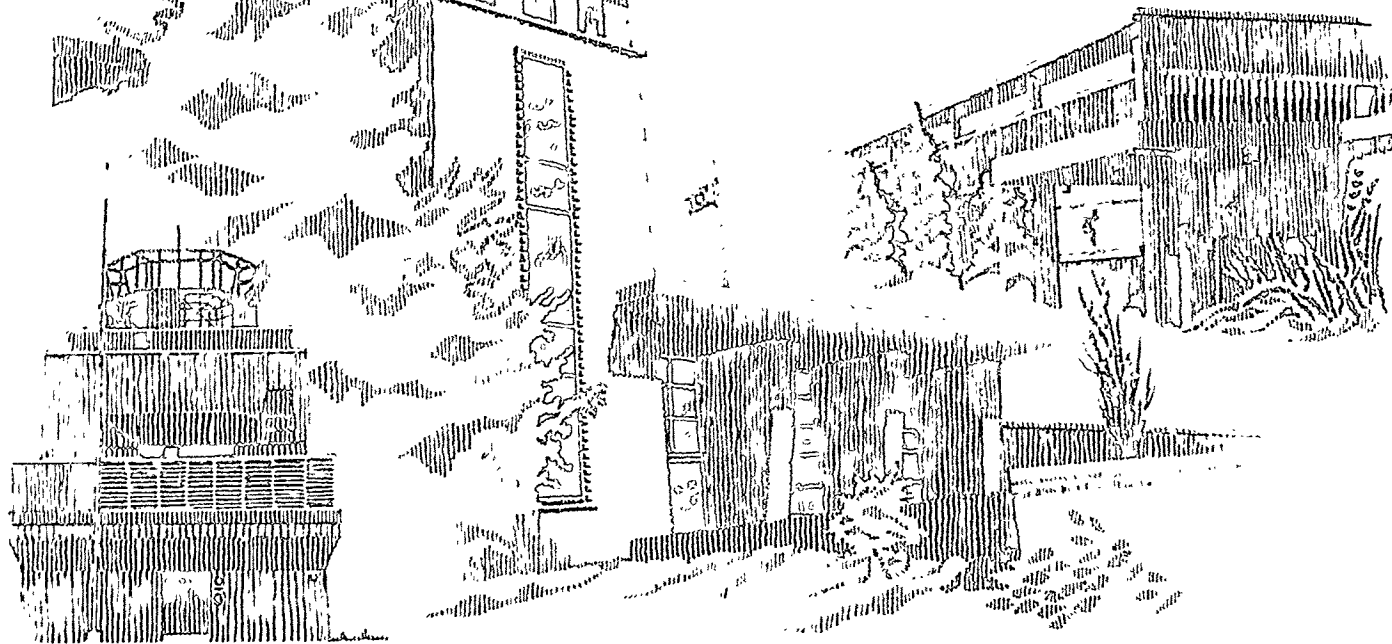
S. J. Glass, J. R. Michael, M. J. Readey, S. I. Wright, D. P. Field

Prepared by  
Sandia National Laboratories  
Albuquerque, New Mexico 87185 and Livermore, California 94550  
for the United States Department of Energy  
under Contract DE-AC04-94AL85000

DISTRIBUTION OF THIS DOCUMENT IS UNLIMITED  
*for*

Approved for public release; distribution is unlimited.

MASTER



Issued by Sandia National Laboratories, operated for the United States Department of Energy by Sandia Corporation.

**NOTICE:** This report was prepared as an account of work sponsored by an agency of the United States Government. Neither the United States Government nor any agency thereof, nor any of their employees, nor any of their contractors, subcontractors, or their employees, makes any warranty, express or implied, or assumes any legal liability or responsibility for the accuracy, completeness, or usefulness of any information, apparatus, product, or process disclosed, or represents that its use would not infringe privately owned rights. Reference herein to any specific commercial product, process, or service by trade name, trademark, manufacturer, or otherwise, does not necessarily constitute or imply its endorsement, recommendation, or favoring by the United States Government, any agency thereof or any of their contractors or subcontractors. The views and opinions expressed herein do not necessarily state or reflect those of the United States Government, any agency thereof or any of their contractors.

Printed in the United States of America. This report has been reproduced directly from the best available copy.

Available to DOE and DOE contractors from  
Office of Scientific and Technical Information  
PO Box 62  
Oak Ridge, TN 37831

Prices available from (615) 576-8401, FTS 626-8401

Available to the public from  
National Technical Information Service  
US Department of Commerce  
5285 Port Royal Rd  
Springfield, VA 22161

NTIS price codes  
Printed copy: A03  
Microfiche copy: A01

## **DISCLAIMER**

**Portions of this document may be illegible  
in electronic image products. Images are  
produced from the best available original  
document.**

## Characterization of Microstructure and Crack Propagation in Alumina Using Orientation Imaging Microscopy (OIM)

S. J. Glass  
Materials Joining  
Sandia National Laboratories  
Albuquerque, NM 87185-0367

J. R. Michael  
Microstructural Characterization  
Sandia National Laboratories  
Albuquerque, NM 87185-1405

M. J. Readey  
Caterpillar Inc.  
Peoria, IL 61656

S. I. Wright and D. P. Field  
TSL, Inc.  
Provo, UT 84604

### Abstract

Conventional studies of structure-property relationships for polycrystalline materials have focused either on descriptions of the morphological aspects of the microstructure, such as grain size and shape, or on the chemistry and structure of individual grain boundaries using transmission electron microscopy (TEM). TEM, while capable of determining the misorientation of adjacent grains, can provide information only for a small number of boundaries. A more complete description of a polycrystal requires the lattice orientations of a statistically significant number of grains, coupled with the morphological aspects, such as grain size and shape. This description can be obtained using a relatively new technique known as orientation imaging microscopy (OIM), which utilizes crystallographic orientation data obtained from Backscattered Electron Kikuchi patterns (BEKP) collected using a scanning electron microscope. This report describes the OIM results for alumina. The results include image quality maps, grain boundary maps, pole figures, and lattice misorientations depicted on MacKenzie plots and in Rodrigues space. High quality BEKP were obtained and the images and data readily reveal the grain morphology, texture, and grain boundary misorientations, including those for cracked boundaries. A larger number of grains should be measured to make statistical comparisons between materials with different processing histories.

*Acknowledgments*

The authors thank Desi Kovar for providing the alumina samples.

## Contents

<b>Executive Summary.....</b>	<b>v</b>	
<b>Introduction.....</b>	<b>1</b>	
<b>Experimental Procedure.....</b>	<b>4</b>	
Sample Processing .....	4	
Sample Preparation for OIM .....	4	
Pattern Collection and Data Analysis.....	4	
<b>Results and Discussion.....</b>	<b>5</b>	
General Features of the Intensity Pole Figure Microtexture Representations and Rodrigues Space Mesotexture Representations.....	11	
5 $\mu\text{m}$ , 99.99% alumina .....	11	
10 $\mu\text{m}$ , 99.99% alumina.....	11	
27 $\mu\text{m}$ , 99.99% alumina.....	11	
4 $\mu\text{m}$ , 99.7% alumina.....	11	
13 $\mu\text{m}$ , 99.7% alumina .....	11	
Misorientations for Cracked Boundaries .....	11	
<b>Conclusions.....</b>	<b>12</b>	
<b>References.....</b>	<b>13</b>	
 <b>Figures.....</b>	 	
1	a) OIM image for the 27 $\mu\text{m}$ , 99.99% alumina sample together with b) a conventional scanning electron microscope micrograph of the same region. The arrow highlights the same grain in both images.....	5
2	Image quality map for the 10 $\mu\text{m}$ , 99.99% alumina sample with darker pixels representing a lower image quality. Arrows highlight a crack that runs from the middle left of the image to the upper right.....	6
3	The OIM image of the 10 $\mu\text{m}$ , 99.99% alumina with the addition of grain boundaries, which are drawn for misorientations between neighboring measurements of greater than 15°. Dots within grains, which produce a chicken wire like appearance, indicate regions whose orientation has been determined with low confidence.....	6
4	The OIM image of the 10 $\mu\text{m}$ , 99.99% alumina sample after a clean-up procedure was used to minimize the presence of ambiguous patterns. The shades in this image are used only to help delineate the grains.....	7
5	The 002 intensity pole figures.....	8
6	The misorientation distributions as represented in MacKenzie plots.....	9
7	The predicted MacKenzie plot of random misorientations for crystals with 3-fold dihedral symmetry.....	10
8	Misorientations displayed in Rodrigues space for the 13 $\mu\text{m}$ , 99.7% alumina sample.....	10
9	The OIM image of the 10 $\mu\text{m}$ , 99.99% alumina sample and the points that were used to determine the distribution of misorientations along the crack it contains.....	12
10	The MacKenzie plot for the misorientations of the crack in Fig. 9. Low angle misorientations represent transgranular fracture.....	12

*Intentionally Left Blank*

## Executive Summary

Conventional studies of structure-property relationships for polycrystalline materials have focused either on descriptions of the morphological aspects of the microstructure, such as grain size and shape, or on the chemistry and structure of individual grain boundaries using transmission electron microscopy (TEM). TEM, while capable of determining the misorientation of adjacent grains, can provide information only for a small number of boundaries. A more complete description of a polycrystal requires the lattice orientations of a statistically significant number of grains, coupled with the morphological aspects, such as grain size and shape. This description can be obtained using a relatively new technique known as orientation imaging microscopy (OIM), which utilizes crystallographic orientation data obtained from Backscattered Electron Kikuchi patterns (BEKP) collected using a scanning electron microscope.

This Laboratory Directed Research and Development (LDRD) project was undertaken to determine the feasibility of using this new microstructural characterization technique on polycrystalline alumina ceramics. If successful, previously unavailable information about the structure of these materials could be used to make improved predictions about their mechanical performance and reliability in applications in numerous weapons' components and as input to and validation of computational models being developed at Sandia for polycrystalline materials.

This report describes the successful implementation of OIM for alumina. The results include image quality maps, grain boundary maps, pole figures, and lattice misorientations depicted on MacKenzie plots and in Rodrigues space. High quality BEKP were obtained for alumina, and the images and data readily reveal the grain morphology, texture, and grain boundary misorientations, including those for cracked boundaries. A larger number of grains should be measured to make statistical comparisons between materials with different processing histories and to determine how the crystallographic misorientation distribution of alumina affects its fracture behavior and reliability.

*Intentionally Left Blank*

# Characterization of Microstructure and Crack Propagation in Alumina Using Orientation Imaging Microscopy (OIM)

## Introduction

This report describes the measurement of microtexture and mesotexture in alumina using a recently developed microstructural characterization technique known as Orientation Imaging Microscopy (OIM). Prior to the development and implementation of this technique there was no way to develop models of structure-property relationships for polycrystalline materials that included information on the texture and microtexture for enough grains to be meaningful. While numerous OIM measurements have been conducted for metals, there have been only a limited number of measurements for ceramic materials and no measurements for materials in which microtexture and mesotexture have been evaluated as a function of grain size and purity. This information is important for the development of improved microstructural evolution and reliability models.

## Background

The mechanical and electrical behavior of a polycrystalline material depends upon the properties of the individual grains, their spatial orientation, and the properties and orientations of the grain boundaries. While relationships between grain size and shape and material properties have been studied extensively, the effects of lattice orientations (microtexture) and misorientations between grains (mesotexture or grain boundary texture) have been difficult to identify because a measurement technique that accounted for a sufficient number of grains to be representative of a complete microstructure was not available. Many studies have reported that the properties of a polycrystal vary as a function of grain size. For example, in many ceramics a transition from intergranular to transgranular fracture occurs as the grain size increases. Explanations for this include grain boundary impurity segregation and microcracking; however, these may be symptoms of the cause of the transition rather than the cause itself. The true cause may be that the distributions of lattice orientations and misorientations are changing as the microstructure evolves. Certain boundaries have a higher mobility than others,<sup>1,2</sup> which may lead to the preferential removal of these boundaries, leaving a microstructure that is less random than it was. If high energy boundaries, which generally correspond to high angle boundaries, are preferentially eliminated, this may lead to a microstructure that has more fracture resistant boundaries with a concomitant increase in the amount of transgranular fracture.<sup>3</sup>

There is mounting evidence that lattice orientations and boundary types in polycrystals play a crucial role in determining the intrinsic response of the material and its overall properties.<sup>4</sup> Special boundaries may dominate the behavior of a material. For example, in Ni<sub>3</sub>Al, low-angle and  $\Sigma 3$  boundaries are strong, whereas high-angle boundaries are prone to cracking.<sup>5</sup> Other properties that are different for special boundaries compared to the general population include impurity segregation,<sup>6</sup> diffusion, mobility, energy, resistivity, and corrosion resistance. The dramatic differences in properties as a function of the misorientations are exemplified by  $\Sigma 3$  boundaries on the 110 zone that have energies of 0.01-0.61 J/m<sup>2</sup>, compared to values of ~ 1 J/m<sup>2</sup> for a totally disordered, general boundary.<sup>7</sup> The implication is that if a polycrystal could be engineered with a high percentage of special boundaries, then there would be an opportunity to enhance the overall properties.<sup>3,8</sup>

The misorientation between two grains is completely described by five parameters, three for the lattice misorientation and two for the boundary normal. It is typically the lattice misorientation that is related to the properties of the grain boundaries, although it is clear that the boundary inclination is also important, especially for special boundaries.<sup>9</sup> A convenient framework for describing the crystallography of the grain boundary is the coincidence site lattice (CSL) model.

Although there is very little information regarding microtexture<sup>10</sup> and mesotexture<sup>4,11</sup> and how they are influenced by processing and microstructural evolution, it is well known that preferred orientation or macrotexture (non random distributions of lattice orientations with respect to the specimen axes) can produce an anisotropic response in polycrystalline materials. In structural materials the anisotropy can be in the elastic properties, fracture toughness, and strength. Macrotexture measurements indicate that directionally-dependent processing techniques, such as hot-pressing and forging, lead to preferred orientations. During hot-pressing, which is the approach used to densify many ceramics, both grain rotation and preferred grain growth can contribute to the development of macrotexture.<sup>12</sup> Strong basal textures are produced in hot-pressed or forged alumina.<sup>13</sup>

Macrotexture measurements are usually made using X-Ray or neutron diffraction techniques, and the results are expressed using the orientation distribution function (ODF). The ODF provides the volume fraction of crystals with a given orientation. Although X-Ray and neutron diffraction macrotexture measurements suggest the presence of a higher than random distribution of special boundaries in many materials, these characterization techniques are unable to provide specific information on the orientation relationship between individual grains (mesotexture or grain boundary texture) or on the relationship between the distribution of lattice orientations and microstructural features, such as grain size and grain shape (microtexture). For example, are specific orientations associated with the large or small grains in the microstructures? Also, small components of macrotexture may be missed, or complementary texture components with similar volume fractions may cancel each other out, producing the effect that no texture is detected. Thus, models based on ODF macrotexture data may not be detailed enough to provide valid structure-property relationships.

Even in the absence of directionally dependent processing and when there is no evidence of macrotexture, microtexture and mesotexture may exist because they are the natural outcome of microstructural evolution. As mentioned earlier, a higher than random frequency of special boundaries may be present after grain growth because certain boundaries are likely to be preferentially eliminated. Certain boundaries have a higher velocity because of their higher mobility and/or the higher driving forces for their migration. This is especially true for materials with a plate-like morphology.<sup>14</sup> The importance of the mesotexture has been noted for both the development of anisotropic microstructures and abnormal grain growth.<sup>15</sup> Similar to the ODF, the misorientation distribution function or MDF has been developed to help characterize the statistical distribution of grain boundary misorientations in a polycrystal.

Techniques for obtaining the lattice orientation data include optical mineralogical techniques, etch pits, back-reflection Laue patterns, electron diffraction in the transmission electron microscope (TEM), electron channeling, X-ray diffraction using a conventional laboratory diffractometer or a synchrotron radiation source, Kossel X-Ray diffraction, and electron backscatter diffraction in the SEM. These techniques are reviewed by Wright.<sup>16</sup> Except for electron backscatter diffraction in the SEM, each technique has limitations that prevent the acquisition of data regarding the effects of lattice orientation and grain misorientation on properties. These limitations include low resolution, unavailability of an appropriate radiation source, sample preparation difficulties, and the inability to study large areas of the specimen.

A fairly recent technique for characterizing lattice orientations makes use of backscattered electron Kikuchi patterns (BEKP). The first observations of these patterns were reported in 1954 and called High-angle Kikuchi patterns by Alam et al.<sup>17</sup> The first use of BEKP in an SEM for lattice orientation determination was in 1973 by Venables and Harland.<sup>18</sup> In order to obtain a BEKP, the incident electron beam is focused and held stationary on a feature of interest on a specimen that is tilted about 70° toward the BEKP detector. Inside the specimen, the electrons are inelastically and elastically scattered; some are scattered at high angles and exit the specimen. Some of these backscattered electrons satisfy the Bragg condition and are diffracted into pairs of cones that can be detected using a suitably placed phosphor screen or photographic film. The cones are imaged as conic sections but appear as parallel sets of straight lines due to the large apex angle of the cones. Interpretation of the pairs of lines, known as Kikuchi bands, allows the specific orientation of the crystal to be determined.<sup>19</sup>

Pioneering work by Dingley, including the introduction of the use of a low light level video camera and on-line computer analysis to aid in the identification of patterns, revealed the potential power of the technique.<sup>20</sup> Substantial progress in the last decade in hardware and software has provided a unique opportunity to interrogate microstructures. Completely automated systems are now available for determining lattice orientations from backscattered electron Kikuchi patterns (BEKPs). More detailed descriptions of the hardware and software routines can be obtained in recent references.<sup>16,21</sup> Presently, a spatial resolution of 200 nm and a precision of 1° can be obtained.<sup>16</sup> Approximately thirty orientations can be determined per minute, allowing hundreds to thousands of grains to be analyzed in a day, depending on the grain size.

Not only does the BEKP technique allow the determination of orientations in a statistically meaningful manner, but it can also be coupled with information about morphological parameters such as grain size and shape. The term that Adams et al. coined for this coupled information is Orientation Imaging Microscopy (OIM).<sup>22</sup> In OIM, the crystallographic orientation is obtained from automatic indexing of BEKPs. The computer controls the electron beam in the SEM so that BEKPs and the corresponding lattice orientation can be obtained at many points on the sample on a user defined grid. In addition to the orientation, the computer records the x,y coordinates, a parameter characterizing the image quality (IQ) of the corresponding BEKP, and a confidence index (CI) describing the confidence the computer has that the indexing algorithm has correctly identified the lattice orientation. An image can then be generated by mapping any of these parameters onto a color or gray scale and shading each point on the data measurement grid accordingly. Such images enable the spatial arrangement of orientation to be graphically displayed providing visual cues to the connection between morphological features of the microstructure and lattice orientation.

To fully utilize the range of information from BEKP data requires statistical measures of the microstructure, such as the ODF and MDF. Plotting both the distribution functions and discrete orientation and misorientation data using a variety of representations can help identify the salient crystallographic elements of the microstructure. In this study we have used several representations of the crystallographic data including pole figures recalculated from ODFs, MacKenzie plots, and discrete plots of misorientation in Rodrigues space.<sup>23</sup> The MacKenzie plot shows only the distribution of the misorientation angle and does not include any information about the axis of rotation.

Quantitative, statistical information on the orientations of thousands of grains in a polycrystal is expected to reveal previously unknown characteristics of materials and to provide a better understanding of structure-property relationships. OIM is still in its infancy in terms of an understanding of its powers and capabilities, the number of materials that remain to be analyzed, and identifying which crystallographic features are most relevant. Once we have gained a better understanding of the range of information available and its relevance, some long-standing questions regarding structure-property relationships may finally be answered.

The objectives of this study were to determine whether useable BEKPs could be obtained for polycrystalline alumina materials and to use OIM to examine microtexture and mesotexture as a function of purity (99.7 and 99.99%) and grain size. We were also interested in examining the distribution of boundary misorientations along cracks in alumina and comparing them to the distribution of boundary misorientations in the bulk. Details regarding the fracture behavior of these alumina materials can be found in recent references.<sup>24,25</sup>

## Experimental Procedure

### Sample Processing

Two commercially available alumina powders (99.7%<sup>i</sup> and >99.99%<sup>ii</sup>) were uniaxially pressed at 28 MPa into disks 25 mm in diameter and approximately 3 mm thick. The disks were subsequently isostatically pressed at 280 MPa. The isopressed density was ~ 57% of the theoretical density, 3.98 g/cm<sup>3</sup>. The disks were buried in a bed of identical powder in high purity alumina crucibles and fired at 1600°C for 5 hr at a heating rate of 5°C/min and a cooling rate of 10°C/min. To increase grain size, specimens were subsequently fired at 1720°C for times up to 48 hr. Quantitative stereology on SEM micrographs provided mean grain sizes ( $d_{avg}$ ) of 5, 10, and 27  $\mu$ m for the 99.99%  $Al_2O_3$ , and 4 and 13  $\mu$ m for the two 99.7%  $Al_2O_3$  materials. The grain size distributions appear to be self-similar as grain size increases, but the distribution is broader for the lower purity material. The mean aspect ratio was ~1.5 for the 99.99%  $Al_2O_3$ , representing a grain shape close to equiaxed for all grain sizes and ~2 for the lower purity alumina, representing a more elongated shape. Densities ranged from 98.6% theoretical density (TD) for the fine-grained 99.99% material to 99.2% TD for the coarse grained 99.99% material and from 98.7 to 98.29% TD for the 99.7%  $Al_2O_3$  materials.

### Sample Preparation for OIM

Conventional metallographic polishing techniques, which consisted of grinding flat with a 9  $\mu$ m fixed diamond wheel at an applied load of 150 N, followed by 9, 6, and 3  $\mu$ m diamond polishing at 150 N, were used to prepare the samples. The final polish was done using colloidal silica for three minutes at an applied load of 100 N. Samples were lightly coated with carbon to prevent charging effects. Coating does not noticeably degrade the backscattered electron Kikuchi patterns.<sup>26</sup>

### Pattern Collection and Data Analysis

The BEKP analyses were performed using a Philips XL30 tungsten source SEM at a voltage of 30 KeV. The beam current was approximately 5 nA. The SEM was equipped with a low-light, silicon-intensified tube (SIT) camera capable of capturing BEKP images at a light level of  $5 \times 10^{-5}$  lux. BEKP data were obtained over a regular hexagonal grid on the surface of each specimen. The scan on the coarse grained alumina ( $d_{avg}=27 \mu$ m) covered an area of 400 $\mu$ mx400 $\mu$ m with a step size of 2  $\mu$ m. The fine grained alumina ( $d_{avg}=5 \mu$ m) was scanned over an area of 200 $\mu$ mx200 $\mu$ m with a step size of 1  $\mu$ m. Alumina was indexed using trigonal crystal symmetry with lattice parameters of  $a=b=4.76 \text{ \AA}$  and  $c=12.99 \text{ \AA}$ . The alumina data sets consisted of approximately 46,000 orientation measurements each. BEKP images were transferred to a Silicon Graphics Indy

<sup>i</sup> A16 SG Alumina, Alcoa Industrial Chemicals, Pittsburgh, PA.

<sup>ii</sup> AKP-50, Sumitomo Chemical Company, New York, NY.

workstation, where TSL's Orientation Imaging Microscopy™ software processed the desired data sets of x-y coordinates, Euler angles, image quality, and confidence index measures.

## Results and Discussion

Useable backscattered electron Kikuchi patterns (BEKP) were obtained from all five alumina samples. Figure 1 shows the OIM image produced for the 27  $\mu\text{m}$ , 99.99% alumina sample together with a conventional scanning electron microscope micrograph of the same area. One grain

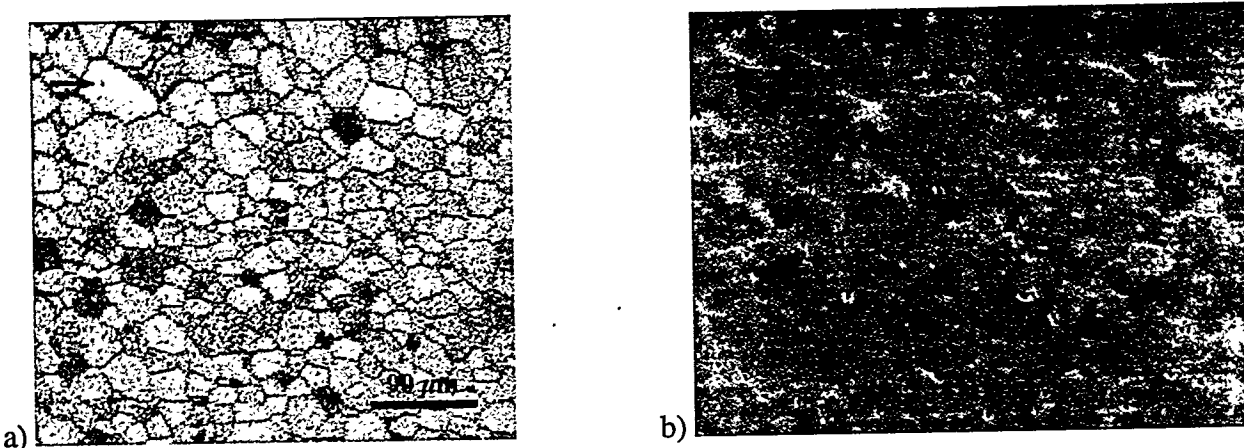


Figure 1. a) OIM image for the 27  $\mu\text{m}$ , 99.99% alumina sample together with b) a conventional scanning electron microscope micrograph of the same region. The arrow highlights the same grain in both images.

is highlighted with an arrow to indicate its position in both images. Note that the sample was not deliberately etched, but grains are apparent in the conventional SEM micrograph because of chemical etching that occurred during the colloidal silica polishing step. One of the advantages of OIM is that no etching of the samples is required to delineate the grains. Grain sizes were calculated from the OIM images and compared to the results obtained in a previous study where standard stereological analyses were performed on conventional SEM micrographs.<sup>24</sup> The average grain size from the OIM image of the largest grain alumina sample was 28  $\mu\text{m}$  compared to 27  $\mu\text{m}$  from the conventional SEM measurements.

Figure 2 is an image quality map for the 10  $\mu\text{m}$ , 99.99% alumina sample with darker pixels representing a lower image quality. The image quality map is determined from the confidence index measured for each pattern, which is a function of diffuseness of the BEKP image. The diffuseness of the image is related to both the orientation and to the perfection of the material. High dislocation densities and surface imperfections, including roughness and contamination, produce more diffuse images. The image quality measure is not normalized for orientation, so a distinct difference in this parameter is seen from grain to grain. Grain boundaries produce a low image quality because measurement points near the grain boundaries are generally affected by the superposed diffraction patterns from the two grains separated by the grain boundary, resulting in a transition area of random noise between the true orientation measurements in the grain interiors. A crack, which also produces a low image quality, runs from the middle left of the image towards the upper right (indicated with arrows). Figure 3 shows the same image with the addition of grain boundaries,

regions of the image appear as if each measurement is a different orientation and give a chicken wire appearance. These are regions of low confidence that are assumed to have been indexed improperly. All such data can be disregarded in the analysis or corrected for by using a clean-up routine that uses a voting procedure to determine the most likely orientation for a given diffraction pattern (described below).

A more detailed analysis of the points contained within the box in Fig. 3, which appear to be part of a single grain, indicate that two orientations are obtained consistently. The fact that the orientations measured within this grain are not the same and that the average confidence index for the grain is low, along with the fact that there are similarly oriented, but scattered measurement points within the grain, suggests that the indexing algorithm may have difficulty properly indexing the diffraction pattern associated with this grain and others that display the same chicken wire appearance. This ambiguity in pattern recognition for alumina needs to be investigated in more detail. While the orientations from these grains seem to be random, there is a possibility that certain orientations are more likely to produce diffraction patterns that produce non-unique indexing solutions.

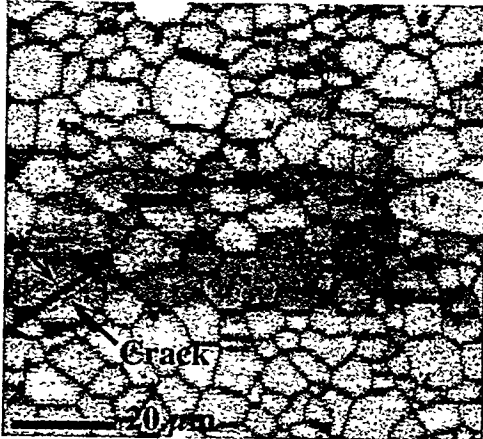


Figure 2. Image quality map for the 10  $\mu\text{m}$ , 99.99% alumina sample with darker pixels representing a lower image quality. Arrows highlight a crack that runs from the middle left of the image to the upper right.

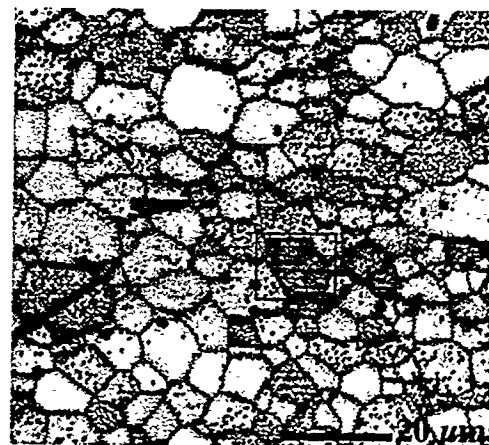


Figure 3. The OIM image of the 10  $\mu\text{m}$ , 99.99% alumina with the addition of grain boundaries, which are drawn for misorientations between neighboring measurements of greater than  $15^\circ$ . Dots within grains, which produce a chicken wire like appearance, indicate regions whose orientation has been determined with low confidence.

This would bias the texture results away from these types of orientations. The data set was processed to ignore data from these types of grains using the following clean-up procedure. When a point is surrounded by three points with the same orientation, its orientation is changed to match the orientation of those three points. Then the data is grouped into grains by grouping neighboring points whose orientation does not differ more than 5 degrees. Finally, grains with less than 25 measurement points per grain were neglected. This procedure results in the image shown in Fig. 4. The shades in this image are not related to the grain orientations in any way but are used to help delineate the grains. The clean-up procedure is not entirely effective in eliminating the unreliable data, but it allows the noise associated with points near grain boundaries to be eliminated, producing a better structure for generating accurate orientation and misorientation distributions.

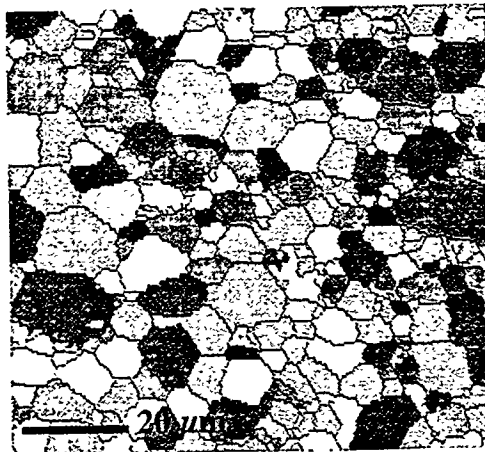


Figure 4. The OIM image of the 10  $\mu\text{m}$ , 99.99% alumina sample after a clean-up procedure was used to minimize the presence of ambiguous patterns. The shades in this image are used only to help delineate the grains.

Figure 5 shows the 002 (using the 3 index notation for hexagonal symmetry) intensity pole figures for each of the alumina samples. The rolling direction (RD) and transverse direction (TD) represent the two directions in the plane of the sample, which is perpendicular to the original uniaxial pressing direction. Figure 6 shows the misorientation distributions as MacKenzie plots, which show the frequencies of given misorientations. The predicted random misorientations for crystals with  $n$ -fold dihedral symmetry (where trigonal is represented by  $n=3$ ) are shown in Fig. 7.<sup>27</sup> Misorientation data can also be represented in Rodrigues space, which is particularly useful for the display of mesotexture because special boundaries can be identified.<sup>19</sup> Misorientations for the 13  $\mu\text{m}$ , 99.7% alumina sample, which appears to exhibit the greatest degree of mesotexture, are shown in Rodrigues space in Fig. 8. Rodrigues space plots for the other samples are not included because of space considerations, but the results are discussed below.

Comparison of the MacKenzie plots in Fig. 6 shows that all samples appear to have a greater frequency of misorientations at angles between 55 and 60° than are indicated in the predicted random distribution in Fig. 7. As discussed earlier, in the alumina crystal structure (trigonal - di-pyramidal), there exist certain orientations for which the solution of the BEKP is ambiguous. We believe that the 60° peak in the plots is an artifact of this indexing difficulty. Other than this anomaly, the data in the MacKenzie plots appear to be close to random. The only distribution that is somewhat different than the rest is that for the 13  $\mu\text{m}$ , 99.7% alumina sample, but it represents a smaller number of grains. Its distribution has relatively more misorientations at angles between 5 and 10°, fewer at angles between 10 and 20°, and more variability in the frequency for angles between 60 and 95°. Its pole figure in Fig. 5 also has the least random texture.

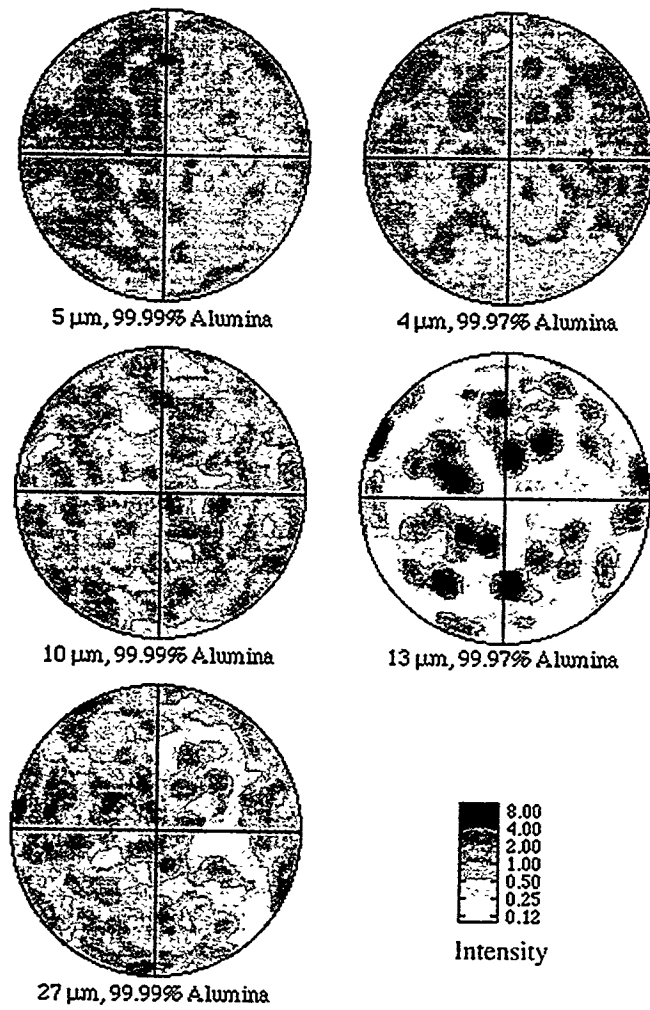
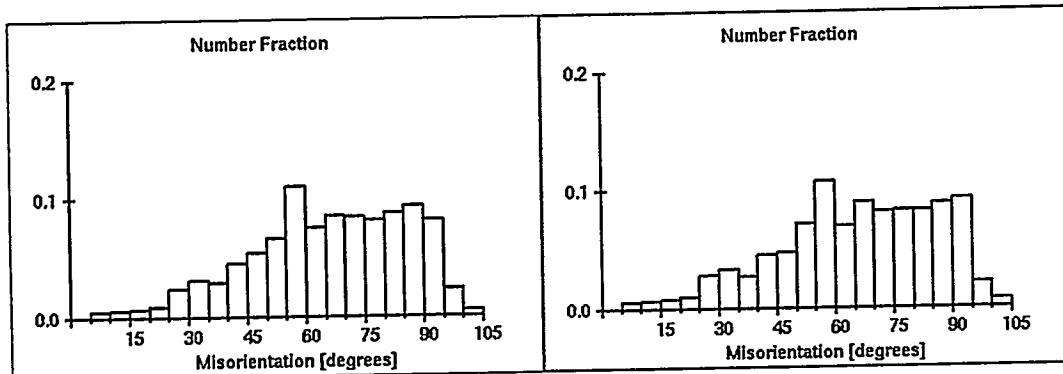
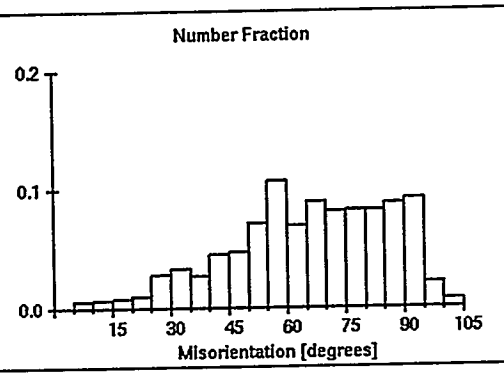


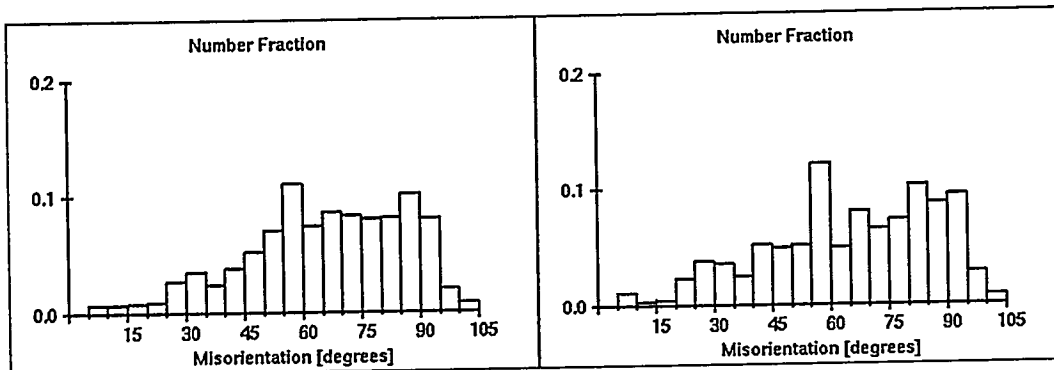
Figure 5. The 002 (3 index notation for trigonal symmetry) intensity pole figures.



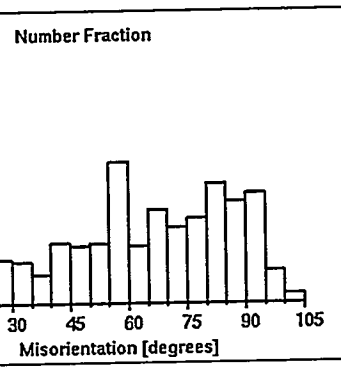
5  $\mu\text{m}$ , 99.99% Alumina



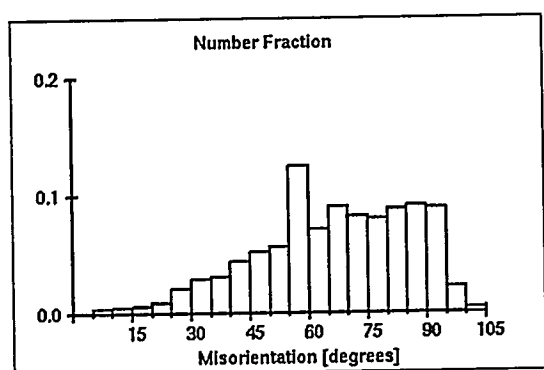
4  $\mu\text{m}$ , 99.7% Alumina



10  $\mu\text{m}$ , 99.99% Alumina



13  $\mu\text{m}$ , 99.7% Alumina



27  $\mu\text{m}$ , 99.99% Alumina

Figure 6. The misorientation distributions as represented in MacKenzie plots.

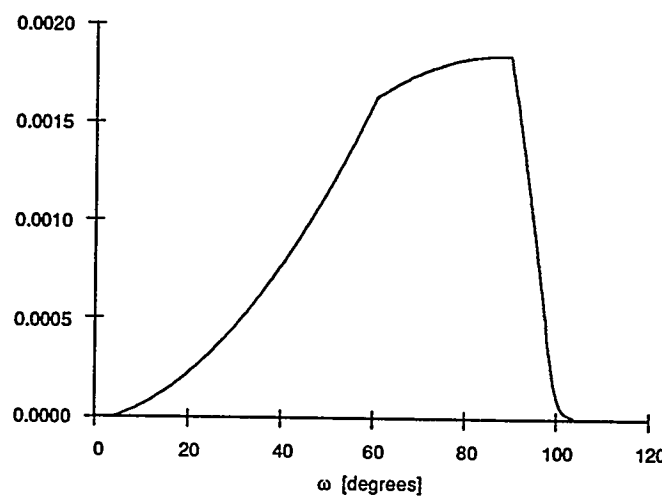


Figure 7. The predicted MacKenzie plot of random misorientations for crystals with 3-fold dihedral symmetry (trigonal).

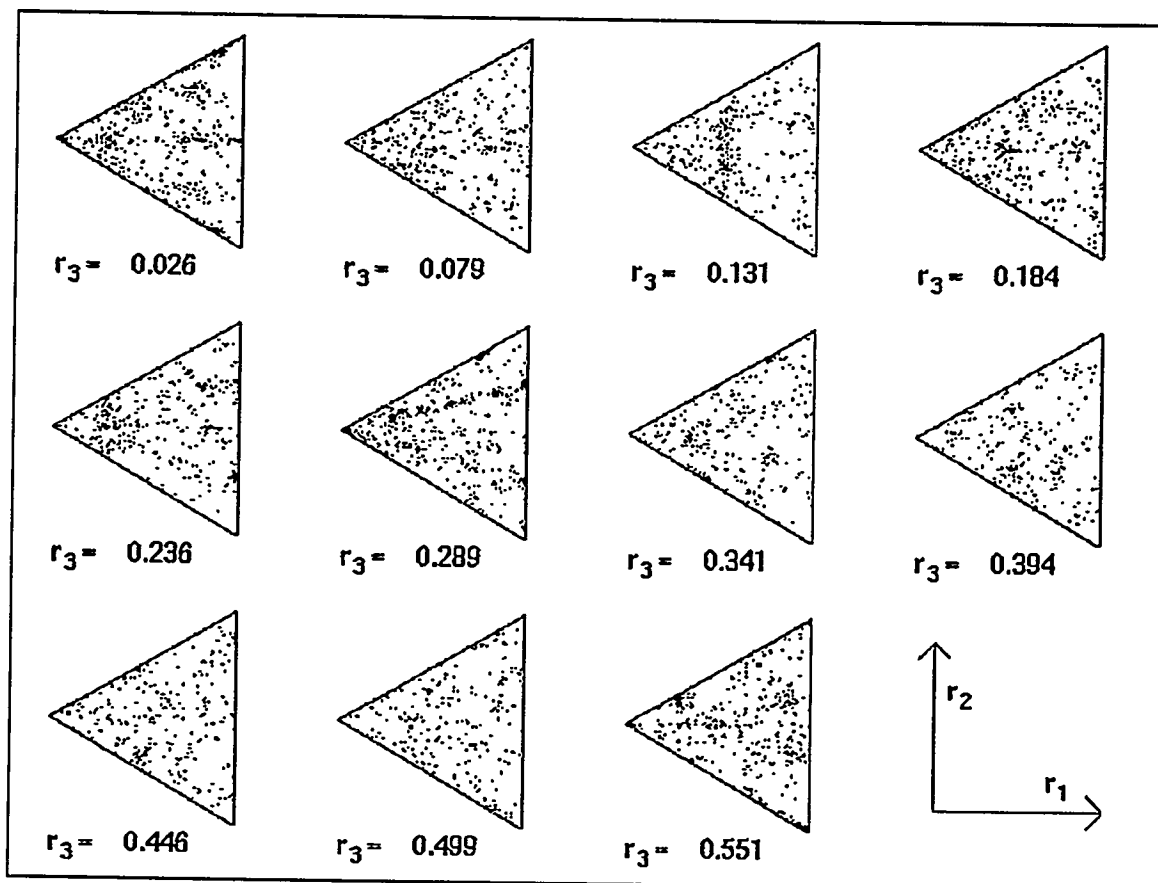


Figure 8. Misorientations displayed in Rodrigues space for the 13  $\mu\text{m}$ , 99.7% alumina sample.

## General Features of the Intensity Pole Figure Microtexture Representations (Fig. 5) and Rodrigues Space Mesotexture Representations

**5  $\mu\text{m}$ , 99.99% alumina.** The texture is quite random as seen by the intensity pole figure for the c-axis. The MacKenzie plot is also fairly random. The misorientations plotted in Rodrigues space are somewhat random but shifted towards c-axis rotations in the distribution (left-hand vertex of each triangle in the space). There are also a number of low angle boundaries (upper-left hand triangle c-axis position).

**10  $\mu\text{m}$ , 99.99% alumina.** The texture is somewhat random, but some clusters appear to be forming. The pole figure shows the c-axis has a weak component as well as a few positions rotated 50-60° off the c-axis. The Rodrigues space plot of misorientations indicates the presence of some low angle and c-axis misorientations but also contains a small cluster at a position of 50° about an a-axis.

**27  $\mu\text{m}$ , 99.99% alumina.** The texture shown in the pole figure is again quite random, and the Rodrigues space plot is similar to that of the 5  $\mu\text{m}$ , 99.99% alumina.

**4  $\mu\text{m}$ , 99.7% alumina.** The texture is weak but has a different character than any of the others. The c-axes are aligning about 70° off the specimen surface normal but only in one general direction. There are some significant features near the rolling direction (RD), and there appears to be some in-plane near c-axis texture.

**13  $\mu\text{m}$ , 99.7% alumina.** The texture in this sample is the strongest of all of the aluminas, but there are also fewer grains in the data set. The distribution tends to be off the c-axis by about 40° in a random direction. The misorientations show a peak in the same position as that described for the 10  $\mu\text{m}$ , 99.99% alumina. Additional components exist, each of which lie near the boundary of the fundamental region, indicating some special but not well defined symmetries.

### Misorientations for Cracked Boundaries

Figure 9 shows the OIM image and the points that were used to determine the distribution of misorientations along a crack in the 10  $\mu\text{m}$ , 99.99% alumina sample. Figure 10 is the MacKenzie plot for these misorientations. Low angle misorientations represent transgranular fracture. Although there appears to be a higher percentage of fracture between grains with large misorientations, relatively few data were used to construct the histogram. Larger numbers of misorientations will need to be measured to identify the true distribution and to determine whether special boundaries, such as low angles and twin boundaries, are absent from the distribution compared to the bulk population. This would provide support for the hypothesis that special boundaries are more fracture resistant. Statistical analyses of misorientation distributions for cracked materials as a function of grain size will also provide information on how the structure of the boundaries is changing as a microstructure evolves.

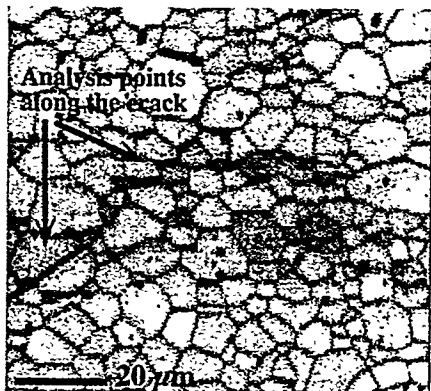


Figure 9. The OIM image of the 10  $\mu\text{m}$ , 99.99% alumina sample and the points that were used to determine the distribution of misorientations along the crack it contains.

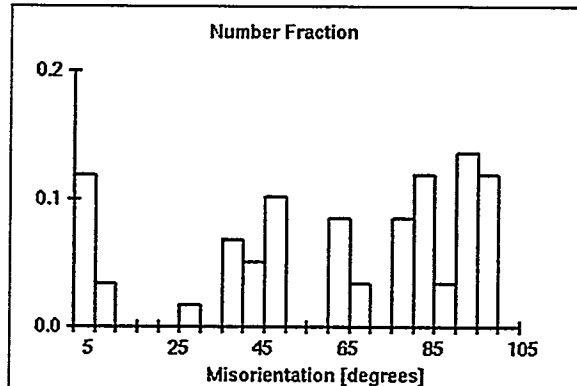


Figure 10. The MacKenzie plot for the misorientations of the crack in Fig. 9. Low angle misorientations represent transgranular fracture.

## Conclusions

Polycrystalline alumina samples were characterized using Orientation Imaging Microscopy (OIM). Good BEKP data were obtained and were used to produce pole figures showing microtexture, and MacKenzie plots and Rodrigues space representations of mesotexture. For the alumina crystal structure, some of the data are unreliable because of the ambiguity in indexing certain orientations. This ambiguity needs to be investigated further. Differences in microtexture and mesotexture in alumina as a function of purity and grain size were subtle but measurable; however, additional measurements will need to be made to provide a more complete picture. Misorientations of cracked boundaries can be measured and compared to the bulk distribution, but larger numbers of misorientations will also need to be obtained to make comparisons. A powerful tool now exists for obtaining meaningful numbers of orientations and misorientations in ceramic materials. This information is expected to provide a better understanding of how these characteristics relate to macroscopic properties such as strength and toughness.

# References

1. V. Randle, B. Ralph, and D. Dingley, The relationship between microtexture and grain boundary parameters, *Acta metall. mater.* 36:267 (1988).
2. G. S. Grest, D. J. Srolovitz, and M. P. Anderson, Computer simulation of grain growth - IV. anisotropic grain boundary energies, *Acta metall. mater.* 33:509 (1985).
3. T. Watanabe, Grain boundary design and control for high temperature materials, *Mater. Sci. Eng.* A166: 11 (1993).
4. V. Randle, Grain assemblage in polycrystals - overview no. 115, *Acta metall. mater.* 42:1769 (1994).
5. H. Lin and D. P. Pope, Weak grain boundaries in Ni<sub>3</sub>Al, *Mater. Sci. Eng.* A192/193:394 (1995).
6. W. Swiatnicki, S. Lartigue-Korinek, and J. Y. Laval, Grain boundary structure and intergranular segregation in Al<sub>2</sub>O<sub>3</sub>, *Acta metall. mater.* 43:795 (1995).
7. V. Randle, An investigation of grain-boundary plane crystallography in polycrystalline nickel, *J. Mater. Sci.* 30:3983 (1995).
8. T. Watanabe, The impact of grain boundary character distribution on fracture in polycrystals, *Mater. Sci. Eng.* A176:39 (1994).
9. A. Garbacz, B. Ralph, and K. J. Kurzydlowski, On the possible correlation between grain size distribution and distribution of CSL boundaries in polycrystals, *Acta metall. mater.* 43:1547 (1995).
10. T. T. Wang, B. L. Adams, and P. R. Morris, Development of orientation coherence in plane-strain deformation, *Met. Trans.* 21A:2223 (1990).
11. V. Randle, Origins of misorientation texture (mesotexture), in: *Textures and Microstructures*, Vol. 14-18, H. J. Bunge, ed., Gordon and Breach Science Publishers SA, United Kingdom (1991).
12. F. Lee and K. J. Bowman, Texture and anisotropy in silicon nitride, *J. Am. Ceram. Soc.* 75:1748 (1992).
13. Y. Ma and K. J. Bowman, Texture in hot-pressed or forged alumina, *J. Am. Ceram. Soc.* 74:2941 (1991).
14. M. S. Sandlin, C. R. Peterson, and K. J. Bowman, Texture measurement on materials containing platelets using stereology, *J. Am. Ceram. Soc.* 77:2127 (1994).
15. J. Rodel and A. M. Glaeser, Anisotropy of grain growth in alumina, *J. Am. Ceram. Soc.* 73:3292 (1990).
16. S. I. Wright, A review of automated orientation imaging microscopy, *J. Comput.-Assist. Microsc.* 5:207 (1993).
17. M. N. Alam, M. Blackman, and D. W. Pashley, High angle Kikuchi patterns, *Proc. Roy. Soc.* 221A:224 (1954).
18. J. A. Venables and C. J. Harland, Electron back-scattering patterns - a new technique for obtaining crystallographic information in the scanning electron microscope, *Phil. Mag. L2*:1193 (1973).
19. V. Randle, *Microtexture Determination and its Applications*, The Institute of Materials, London (1992).
20. D. J. Dingley, A comparison of diffraction techniques for the SEM, *Scanning Electron Microsc.* IV:273 (1981).
21. K. Kunze, S. I. Wright, B. L. Adams, and D. J. Dingley, Advances in automatic EBSP single orientation measurements, in: *Textures and Microstructures*, B. L. Adams and H. Weiland, ed., Gordon and Breach Science Publishers SA, United Kingdom (1993).
22. B. L. Adams, S. I. Wright, and K. Kunze, Orientation imaging: the emergence of a new microscopy, *Metall. Trans. A*, 24A:819 (1993).
23. F. C. Frank, Orientation mapping, *Metall. Trans. A*, 19A:403 (1988).
24. D. Kovar and M. J. Readey, Role of grain size in strength variability of alumina, *J. Am. Ceram. Soc.* 77:1928 (1994).
25. D. Kovar, *The Role of Microstructure on the Mechanical Reliability of Alumina Ceramics*, Ph.D. Thesis, Carnegie Mellon University (1995).
26. J. R. Michael and R. P. Goehner, Advances in backscattered-electron Kikuchi patterns for crystallographic phase identification, in: *Proc. 52nd Annual Meeting*, G. W. Bailey and A. J. Garratt-Reed, ed., Microscopy Society of America (1994).
27. A. Morawiecz and D. Field, Misorientation angle distribution of randomly oriented symmetric objects, submitted to *J. Appl. Cryst.* (1996).

DISTRIBUTION:

1	M. J. Readey Caterpillar Inc. Peoria, IL 61656
2	S. I. Wright and D. P. Field TSL, Inc. Provo, UT 84604
1	MS1434      G. Pike, 1802
1	MS0367      B. Damkroger, 1833
5	MS0367      S. J. Glass, 1833
1	MS1405      R. Goehner, 1822
3	MS1405      J. R. Michael, 1822
1	MS0188      C. E. Meyers, 4523 (LDRD office)
1	MS9018      Central Technical Files, 8523-2
5	0899      Technical Library, 4414
2	0619      Review and Approval Desk, 12630 For DOE/OSTI